Controlling cell shape on hydrogels using lift-off protein patterning

PLOS ONE

RESEARCH ARTICLE

Controlling cell shape on hydrogels using lift-off protein patterning

Jens Moeller[1☯], Aleksandra K. Denisin[1,2☯], Joo Yong Sim[1], Robin E. Wilson[1], Alexandre J. S. Ribeiro[1], Beth L. Pruitt[1,2,3,4]*

1 Department of Mechanical Engineering, Stanford University, Stanford, California, United States of America, **2** Department of Bioengineering, Stanford University, Stanford, California, United States of America, **3** Stanford Cardiovascular Institute, Stanford University, Stanford, California, United States of America, **4** Department of Molecular and Cellular Physiology, Stanford University School of Medicine, Stanford, California, United States of America

☯ These authors contributed equally to this work.
* pruitt@stanford.edu

Citation: Moeller J, Denisin AK, Sim JY, Wilson RE, Ribeiro AJS, Pruitt BL (2018) Controlling cell shape on hydrogels using lift-off protein patterning. PLoS ONE 13(1): e0189901. https://doi.org/10.1371/journal.pone.0189901

Editor: Nic D. Leipzig, The University of Akron, UNITED STATES

Received: August 15, 2017

Accepted: December 4, 2017

Published: January 3, 2018

Data Availability Statement: All relevant data are within the paper and its Supporting Information files.

Funding: This project was supported in part by the National Science Foundation (EFRI-MIKS 1136790, CMMI 1662431, ECCS-1542152), National Institutes of Health (R01EB006745, 1R21HL13099301). The authors are grateful for graduate and post-doctoral research fellowships from the National Science Foundation, ILJU Foundation, Stanford BioX, Stanford Office of the Vice Provost for Graduate Education, American

Abstract

Polyacrylamide gels functionalized with extracellular matrix proteins are commonly used as cell culture platforms to evaluate the combined effects of extracellular matrix composition, cell geometry and substrate rigidity on cell physiology. For this purpose, protein transfer onto the surface of polyacrylamide hydrogels must result in geometrically well-resolved micropatterns with homogeneous protein distribution. Yet the outcomes of micropatterning methods have not been pairwise evaluated against these criteria. We report a high-fidelity photoresist lift-off patterning method to pattern ECM proteins on polyacrylamide hydrogels with elastic moduli ranging from 5 to 25 kPa. We directly compare the protein transfer efficiency and pattern geometrical accuracy of this protocol to the widely used microcontact printing method. Lift-off patterning achieves higher protein transfer efficiency, increases pattern accuracy, increases pattern yield, and reduces variability of these factors within arrays of patterns as it bypasses the drying and transfer steps of microcontact printing. We demonstrate that lift-off patterned hydrogels successfully control cell size and shape and enable long-term imaging of actin intracellular structure and lamellipodia dynamics when we culture epithelial cells on these substrates.

Introduction

Cell culture substrates patterned with extracellular matrix (ECM) are widely used to mimic the spatial organization and rigidity of the *in vivo* cell microenvironment *in vitro*. These cell culture platforms enable reductionist studies of the mechanobiology of healthy and diseased tissues under physiological stiffness conditions [1]. Specifically, polyacrylamide (PAAm) hydrogels are commonly used because these substrates can be functionalized with ECM proteins and tuned in their mechanical properties to replicate different tissue stiffness ranging from ~0.1 kPa to ~40 kPa [2]. Yet techniques for patterning proteins on PAAm have lacked quantitative assessment, which is critical for developing and comparing protocols to reliably

Heart Association, and Stanford Graduate Fellowship. The funders had no role in study design, data collection and analysis, decision to publish, or preparation of the manuscript.

Competing interests: The authors have declared that no competing interests exist.

restrict cells to user-defined shapes. The spatial resolution and accuracy of the protein patterns will directly impact the cellular response which is of particular importance for mechanobiological studies on the organization and force transduction within the actin cytoskeleton [3] and cellular adhesions [4].

Broadly, two main strategies exist to pattern ECM on PAAm gels (reviewed in [5]): i) selective activation of the gels for covalent attachment of proteins to activated regions (e.g. direct surface functionalization using UV-reactive sulfo-SANPAH crosslinkers [2] or polymerizing N-hydroxyacrylamide into the hydrogel surface [6]) and ii) co-polymerization of ECM proteins into the gels during gelation through direct contact of the acrylamide precursor mix with a protein-patterned coverslip. The first method, direct surface functionalization, uses expensive functionalization reagents and also depends on reagent quality and reaction time as the chemicals are unstable in aqueous media and in the presence of oxygen [5]. The method of co-polymerizing ECM proteins relies on patterning glass coverslips with protein and placing them in direct contact with the hydrogel during polymerization. Although the detailed molecular mechanism of protein incorporation into the polymerizing gel is unknown, this method has successfully been applied to functionalize hydrogels with a variety of ECM proteins [7–9].

Protein patterns on glass coverslips are often created by microcontact printing (μCP) using elastomeric 'stamps' [10]. μCP involves casting polydimethylsiloxane (PDMS) on microfabricated master structures created by photolithography to create stamps by replica molding [11]. Most groups use μCP since PDMS casting and contact printing protocols are straightforward once the master structures on silicon wafers are made [7, 12, 13]. However, μCP relies on the transfer of dried proteins from a deformable PDMS stamp and thus the accuracy, resolution, and pattern design are limited and critically depend on the PDMS stamp preparation and handling [14–16]. PDMS can also be micromachined to create a stencil which can be used to selectively adsorb proteins to specific regions of the glass coverslip and keep proteins hydrated throughout the process [17, 18], but the fabrication of a high-resolution stencil requires reactive ion etching which is not available to all laboratories [19] and stencil alignment and conformal contact with the substrate is required for successful protein patterning. A technique similar to μCP called "stamp-off" allows for proteins to first be adsorbed on a surface and then selectively being removed by a PDMS stamp placed in contact with the substrate [20]. While stamp-off can enable patterning multiple proteins, it still suffers from the same lateral size limitations as μCP. To improve the accuracy of μCP, alternative nanopatterning methods have been developed for patterning proteins on substrates (reviewed in [21]). For example, dip-pen nanolithography, AFM-based patterning, and nanografting enable direct writing of proteins on flat, solid substrates with nanometer precision [22]. However, these nanopatterning methods are serial and have not been used to directly functionalize hydrogels.

The challenge of serial patterning can be overcome using approaches to pattern protein features over large areas in parallel using a molecular adlayer to define biopassive regions and backfilling exposed regions with protein. Biopassive, 'non-fouling' Poly(l-lysine)-graft-poly (ethylene glycol) (PLL-g-PEG) copolymers can be used to control protein adsorption to engineered substrates [23, 24]. To pattern proteins on glass, PLL-g-PEG can then be selectively oxidized by deep UV irradiation through a photomask or via projection lithography [25, 26]. Such patterns can subsequently be transferred to a hydrogel [9] thereby decoupling pattern generation from hydrogel functionalization. Those methods however require either access to a collimated deep UV light source or a UV projection system, which are not readily available in most laboratories. Further, the PLL-g-PEG layer must either be dried prior to the UV irradiation, which requires a rehydration step prior to protein incubation [25], or a photoinitiator must be added during the UV exposure step that has to be removed completely to re-establish the biopassive properties of the adlayer [26]. Another method using PLL-g-PEG involves

creating a sacrificial mask on glass and uncovering the protected regions for later incubation steps. In combination with reactive ion etching, Falconnet and colleagues nanoimprinted a poly(methyl methacrylate) (PMMA) film on a glass coverslip, incubated the substrate with a biotinylated PLL-g-PEG copolymer to facilitate the selective binding of avidin-functionalized proteins, and lifted off the nanoimprinted film prior to backfill with biopassive PLL-g-PEG to achieve 100 nm features [27]. Nanoimprinting and reactive ion etching can thus be used in tandem with blocking of nonspecific protein adsorption using biopassive polymers, e.g. PLL-g-PEG, to produce nanometer-scale features on large areas but the process is complex and requires microfabrication equipment not readily available in many laboratories.

In this work, we present a photoresist lift-off patterning (LOP) method to control the shape of cells on PAAm hydrogels with high fidelity. Our method integrates advances in: i) contact photolithography and photoresist lift-off widely used in the semiconductor and microfabrication industry [28], ii) the molecular assembly and patterning of biopassive PLL-g-PEG coatings on glass[29–31], and iii) the protein transfer from glass to PAAm hydrogels [12].

We create protein-patterned glass coverslips by photoresist lift-off-assisted patterning of PLL-g-PEG and transfer the protein pattern to PAAm gel surfaces by co-polymerization. To demonstrate the utility of this approach, we successfully controlled the shape of MDCK cells cultured on patterned hydrogels and followed the cells' cytoskeletal and membrane dynamics. We benchmark the LOP technique to the widely used μCP across a range of physiologically relevant hydrogel stiffness (5 kPa, 10 kPa and 25 kPa) and analyze the pattern accuracy and transfer efficiency from the glass to the PAAm gel. We find that the LOP protocol improves both the pattern transfer efficiency and the pattern accuracy, thereby reducing the pattern variability and increasing the predictability of the engineered *in vitro* cell culture models.

Materials and methods

Photoresist lift-off assisted patterning of ECM proteins (LOP)

ECM patterned glass coverslips were fabricated by photoresist lift-off (see process flow in Fig 1, full protocol in S1 Text). We cleaned coverslips with acetone, isopropanol, and water, followed by thoroughly drying them on a hot plate. We then spin-coated S1818 photoresist (Microchem) on coverslips using standard contact photolithography and photopatterned the 2μm thick resist layer (40–50 mJ/cm^2 at 365 nm, OAI Instruments) (Fig 1A and 1B). Following plasma activation, we incubated the S1818 patterned glass coverslips with 0.1 mg/ml (poly(l-lysine)-graft-poly(ethylene glycol) (PLL(20)-g[3.5]-PEG(2), SuSoS AG) in PBS (pH 7.4) for one hour to allow for self-assembly of the densely packed, biopassive PLL-g-PEG polymeric brush adlayer on the exposed surface areas of the glass substrate. The PLL(20)-g[3.5]-PEG(2) copolymer comprises of linear PEG chains (M_w = 2 kDa) grafted to a PLL backbone (M_w = 20 kDa) at a grafting ratio g = 3.5 [23]. Non-adsorbed PLL-g-PEG was removed by washing in PBS (pH 7.4). After photoresist lift-off in 1-methyl-2-pyrrolidone (NMP, Sigma 328634), we backfilled the PLL-g-PEG patterns with 100 μg/ml of Oregon Green-488 or Alexa Fluor 568-labeled gelatin solution in PBS pH 7.4 for 1 hour in the dark (Thermo Scientific, G13186, A10238) (Fig 1C–1E). The slides were washed thoroughly with DI water and excess liquid was removed by blotting on filter paper immediately prior to gel transfer. We chose gelatin, hydrolyzed collagen I, as a model ECM protein to mimic the epithelial basement membrane because the Arg-Gly-Asp (RGD) sequence that is critical for cell adhesion, migration and proliferation is preserved [32]. Gelatin, in contrast to collagen I, is available commercially with fluorescent labels or can be functionalized with standard protein labeling kits.

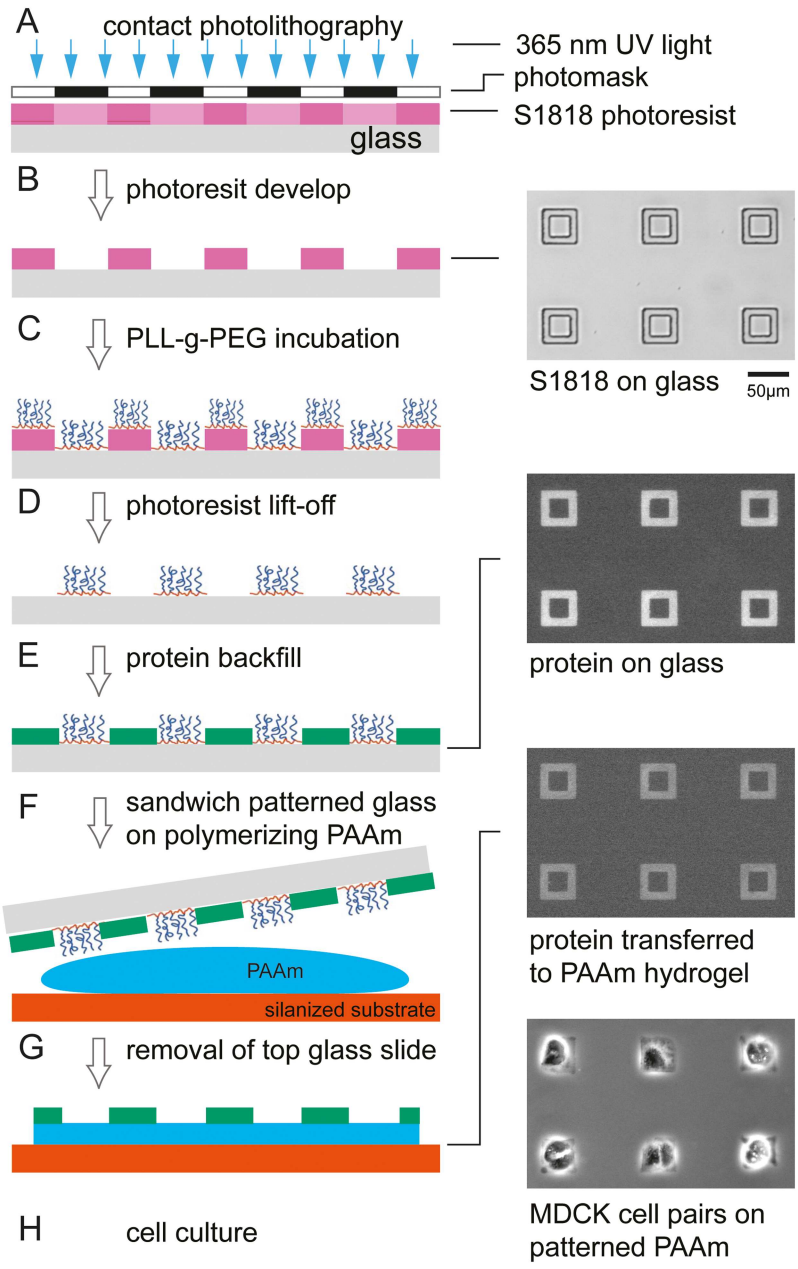

Fig 1. LOP fabrication of protein patterns on polyacrylamide gels. (A,B) Photoresist patterns are fabricated by standard contact photolithography on glass coverslips. Inset at right shows array of S1818 photoresist features after development. (C) Unspecific protein adhesion to the resist-patterned coverslip is blocked by incubating with biopassive PLL(20)-g[3.5]-PEG(2) copolymer. (D,E) Following photoresist lift-off, the resulting PLL-g-PEG pattern is backfilled with the ECM protein of interest. Inset at right shows a fluorescence micrograph of labeled gelatin on glass after backfill. (F) To transfer the protein pattern to the PAAm gel, the gel is polymerized between the protein patterned glass coverslip and a silanized coverslip. (G) After gel polymerization, the top coverslip is removed from the PAAm gel. Inset at right shows a fluorescence micrograph of a labeled protein transferred to a PAAm gel. (H) Inset at right shows pairs of epithelial cells on the patterned PAAm gel restricting the geometry of the protein functionalized regions.

https://doi.org/10.1371/journal.pone.0189901.g001

Microcontact printing of ECM proteins (μCP)

We prepared PDMS stamps by casting Sylgard 184 PDMS (10:1 base to curing agent, Dow Corning) in a 9 μm deep mold microfabricated by standard photolithography using SU-8

negative resist [11]. We incubated the PDMS stamps (1 cm^2 squared stamps with 45 μm^2 patterns with 80 μm spacing) with 100 μg/ml fluorescently labeled gelatin solution for one hour in the dark. Following protein incubation, we aspirated excess protein solution and dried the stamps gently using low nitrogen gas flow. Prior to μCP, we cleaned glass coverslips with 2% v/v Hellmanex solution (Hellma Analytics) in DI water for at least 30 minutes. We then rinsed the coverslips 5 times with DI water and dried them with compressed air prior to stamping. We put the PDMS stamps in contact with the cleaned coverslips for 5 minutes and removed the stamps by carefully forcing a tweezer between the coverslip and the edge of the stamp.

Preparation of ECM patterned polyacrylamide gels

We transferred the protein patterns from the glass coverslip to the surface of PAAm gel for both the LOP and μCP protocols by co-polymerization (Fig 1F–1H). Polyacrylamide gels of varying stiffness were polymerized between the protein patterned glass coverslip and a silanized bottom coverslip. The bottom coverslip was silanized to ensure covalent bonding of gels to this bottom glass layer, following a method by Guo and colleagues [33]. Briefly, 30 μL of working solution (3 μl bind-silane (3-methacryloxypropyl-trimethoxysilane, Sigma-Aldrich, M6514), 950 μL 95% ethanol, and 50 μL of glacial acetic acid) were applied to the coverslip, allowed to incubate for 5 min, and then rinsed with ethanol and dried in a desiccator.

Polyacrylamide gels of three different stiffness were used for experiments: 5 kPa, 10 kPa, and 25 kPa as determined by Tse and Engler [2]. MilliQ water, acrylamide (0.5 g/mL stock, Sigma-Aldrich, 01696 FLUKA, 71.08g/mol), and bis-acrylamide (0.025 g/mL stock, Sigma-Aldrich, 146072, 154.17 g/mol) were combined to yield 5% w/v acrylamide and 0.15% w/v bis-acrylamide for 5 kPa gels, 10% w/v acrylamide and 0.1% w/v bis-acrylamide for 10 kPa gels, and 10% w/v acrylamide and 0.25% w/v bis-acrylamide for 25 kPa gels. The precursor solution was degassed in a vacuum desiccator for 1 hr. To initiate gelation, 5 μL of 10% w/v ammonium persulfate (APS, Sigma-Aldrich, A9164) was added to ~995 μL of gel precursor solution followed by 0.5 μL of N,N,N′,N′-Tetramethylethylenediamine accelerator (TEMED, Sigma-Aldrich, 411019). We mixed the solutions by gentle pipetting, dispersed 50 μL of the solution on the activated coverslip, and then placed the protein-functionalized coverslip on top, creating a sandwich (Fig 1F). Gels were left undisturbed at room temperature for 30 minutes to polymerize. After polymerization, the gels were immersed in PBS for at least 1 hour and the glass coverslip was removed from the top of the gels (Fig 1G).

Analysis of pattern transfer efficiency

To assess the protein transfer efficiency from the patterned glass coverslip onto the PAAm gel, we imaged the coverslips before transfer and compared it to the resulting patterns on the PAAm gel surface after gelation and coverslip removal using the same microscope image acquisition parameters (1 second exposure, images of 1 series acquired at the same day to avoid variability in lamp power). Prior to imaging, we avoided photobleaching by keeping samples in the dark. Our patterns were arranged in labelled arrays so we decreased photobleaching by exposing each area to light only when focusing the image and during image capture. All acquired images were processed by ImageJ software (http://rsb.info.nih.gov/ij/). We analyzed 150 individual patterned features by measuring the difference between the same feature on the coverslip before and after transfer, using the cvMatch_Template ImageJ plugin [34]. The average background signal was determined outside the protein pattern and subtracted for each image. We measured the average pixel intensity within a region of interest defined as our theoretical patterning shape and calculated the transfer efficiency as the average

intensity of the protein pattern on the gel image divided by the average intensity of the pattern on the coverslip.

Analysis of the geometric accuracy of protein patterning

To compare the accuracy of patterns generated by LOP and μCP, we calculated the cross-correlation coefficient between the theoretical pattern shape and the binarized patterned features using the *corr2* function in Matlab (R2014b, Mathworks). The binarized stacks (n = 150 patterns) were created with ImageJ by de-noising the images using the built-in despeckle function followed by automated binarization of each pattern using Otsu thresholding. Profile column average plots were analyzed from the binarized pattern stacks using ImageJ. To perform yield analysis, we selected around 389–416 features for each gel stiffness type, created a montage, and then used cross correlation with a threshold of 0.84 to find acceptable features. We divided the number of acceptable features by the total number of features analyzed for each gel stiffness to calculate the yield.

Analysis of surface energy using water contact angle

We used a contact angle goniometer (Rame-Hart 290) to measure the hydrophilicity of substrates used in LOP and μCP. We dispensed 4 μl of deionized water on the surface, equilibrated for 1 minute at room temperature before taking a photograph of the water contact angle to standardize between measurements and ensure equal evaporation of the liquid. We evaluated the water contact angle of PLL-g-PEG coated glass coverslips before and after polymerization of 25 kPa PAAm gels. Polymerized gels were incubated with PBS overnight at 4˚C before dissociating the top coverslip and performing the water contact angle measurements. We calculated the contact angle using the DropShape ImageJ plugin [35]. Water contact angle measurements are a direct read-out of the surface energy and thus can provide insights of the conformation states of the proteins during both patterning processes.

Cell culture

Madin-Darby Canine Kidney (MDCK) type II G cells were transfected with LifeAct-GFP (ibidi, 60101) using the Amaxa Biosystem Nucleofector II system and transfection kit (Lonza, VCA-1005). The LifeAct-GFP MDCK cells were maintained in low glucose DMEM (Invitrogen, 11885) containing 1 g/l sodium bicarbonate, 1% Penicillin-Streptomycin (PenStrep, ThermoFisher, 15140122), 0.5 mg/ml G418 selection reagent (Sigma-Aldrich, G418-RO Roche), and supplemented with 10% (vol/vol) fetal bovine serum (FBS). 25 kPa PAAm gels patterned with 100 μg/ml collagen I (Gibco, A1048301) mixed with 20 μg/ml Alexa Fluor 568 labeled gelatin were cast into Mattek dishes (14 mm glass, Mattek P35G-0.170-14-C). MDCK cells were trypsinized and seeded on the PAAm gels for 16 hours before imaging experiments. Prior to imaging, the media was replaced to low glucose DMEM with no phenol red (ThermoFisher, 11054001) and supplemented with 1% PenStrep, 10% FBS, and 25 mM HEPES buffer. Cells were imaged on a Leica DMI6000B microscope with heated incubation unit at 5 minute intervals using a 40x air objective, NA = 0.6.

Results

We compare the LOP and μCP methods by analyzing the efficiency of protein transfer from the surface of coverslips onto the surface of PAAm gels (Fig 2) and the geometrical accuracy of the created patterns (Fig 3). We use a square 'frame' pattern shape to compare how both protocols resolve corners and edges of a complex shape. We show pattern arrays of glass and PAAm

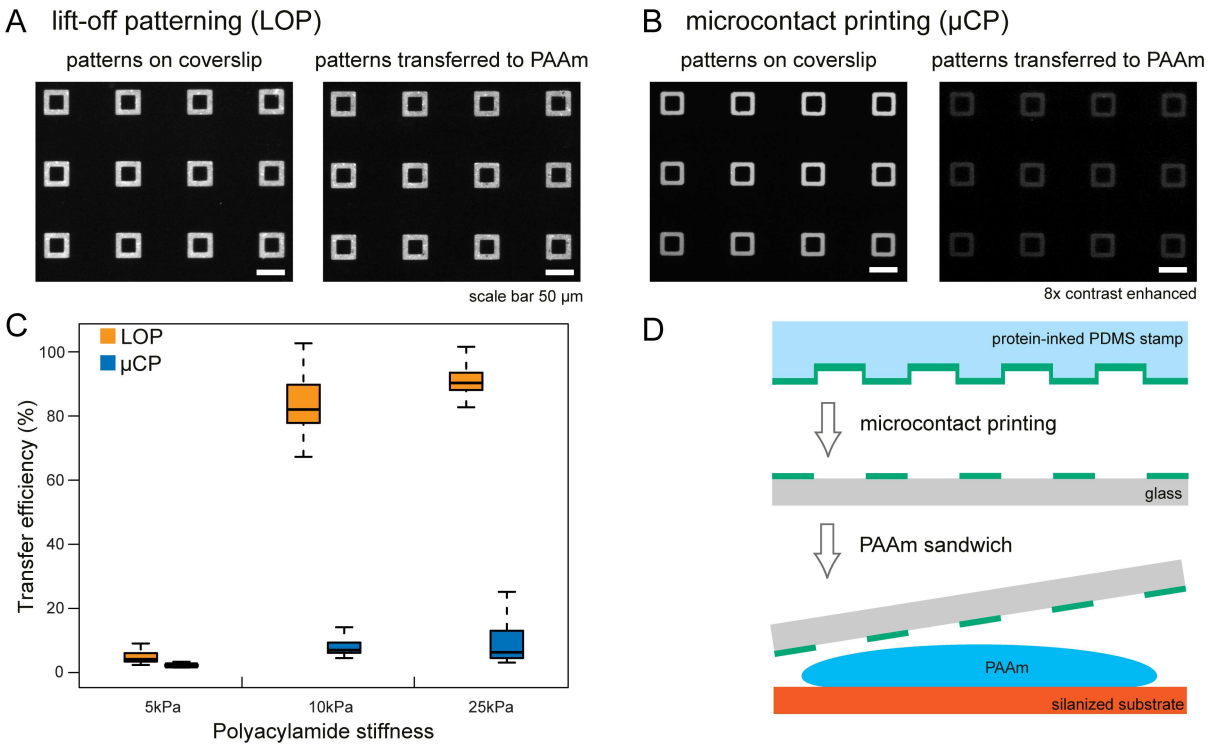

Fig 2. Quantification of protein transfer efficiency to PAAm gels of varying stiffness. (A,B) Arrays of 45 μm^2 square protein patterns on 25 kPa PAAm gels created by LOP and μCP before and after transfer to gel surface. (C) Quantification of protein transfer efficiency from glass coverslips to PAAm gel of varying stiffness. Differences between LOP and μCP for each stiffness are statistically significant (p-value < 2.2E-16, Mann-Whitney-Wilcoxon test). Substantially more protein is transferred from patterns created by photoresist lift-off. Data are represented as box plots. The median, 1st and 3rd quartile, and minimum and maximum values are shown, n = 150 for each method and stiffness shown. (D) Overview of μCP method to pattern proteins on PAAm gels.

https://doi.org/10.1371/journal.pone.0189901.g002

samples normalized for contrast to aid visual comparison of the transfer efficiency for LOP and μCP techniques in Fig 2A and 2B.

Protein patterns created by the LOP method are transferred more efficiently from the coverslips to gels for all gel stiffness we tested (Fig 2C). We find significant differences in transfer efficiency between LOP and μCP when comparing both protocols at each stiffness (p-value $<$ 2.2E-16 using the Mann-Whitney-Wilcoxon to compare the 5 kPa, 10 kPa, and 25 kPa PAAm gel samples). However, the protein transfer efficiency in both methods is considerably lower for 5 kPa when compared to 10 kPa and 25 kPa PAAm gels. To explain this observation, we analyzed and compared the size properties of gelatin and polyacrylamide gel formulations used in this study to those commonly used in mechanobiology and electrophoresis (see S1 Text). The 10 kPa and 25 kPa gel formulations we use contain 10% total polymer which is twice that of the 5 kPa gel formulation (5%). Due to the lower total polymer content, we hypothesize that fewer sites are available for protein integration during polymerization in the 5 kPa gels. This effect is independent of the patterning technique and thus can be a limiting factor for the protein functionalization of soft polyacrylamide gels.

To evaluate the accuracy of the features transferred to PAAm gels, we compare the corners of the square frame patterns for both protocols (Fig 3A) and show the difference between the actual and theoretical shape (Fig 3B). Protein patterns created by LOP exhibit greater definition in the pattern edges and corners than protein patterns created by μCP. Cross-correlation analysis of the patterns compared to the theoretical pattern shape on the photomask shows

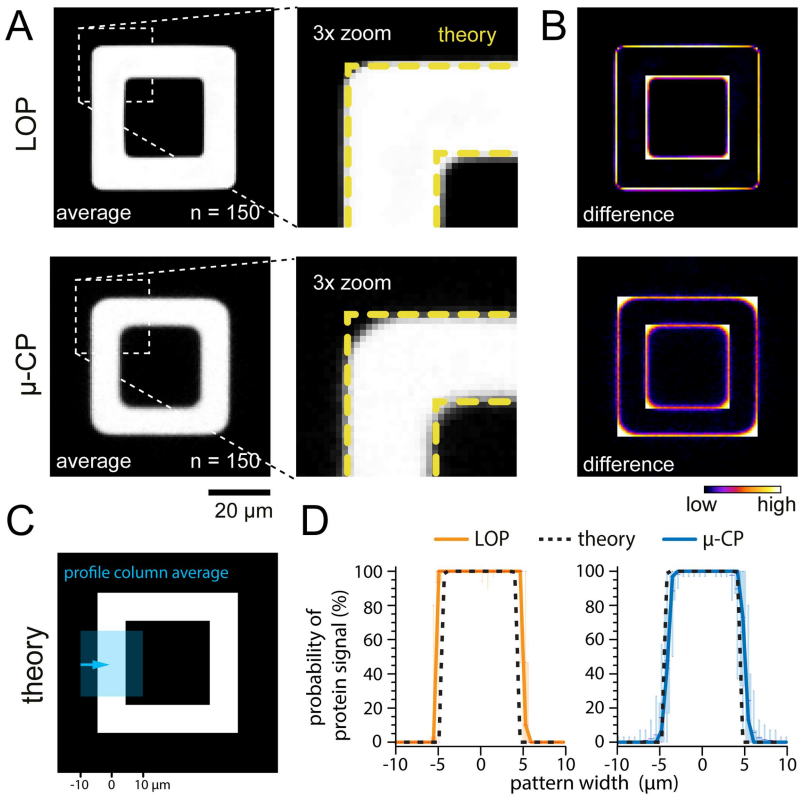

Fig 3. Comparison of pattern accuracy between LOP and μCP methods. (A) Average images of 150 binarized protein patterns created by LOP and μCP on 25 kPa gels. (B) Difference images calculated by comparing the average images and the theoretical pattern mask. Edges and corners are resolved substantially better in patterns created by LOP. (C) Theoretical pattern shape with a region highlighted corresponding to where profile column average scans were taken. (D) Profile column average scans across 150 binarized patterns show that the variation in protein signal at the pattern edges is strongly reduced in LOP patterns. Plotted are the median (line), 1st / 3rd quartile (box) and 5–95% (whisker) of the probability of protein present across the pattern width.

https://doi.org/10.1371/journal.pone.0189901.g003

that LOP results in patterns that more accurately recapitulate the theoretical shape. Correlation coefficients are as follows (n = 150 patterns; mean +/- standard deviation): μCP (5, 10, 25 kPa): 0.84±0.05; 0.87±0.02; 0.89±0.02; LOP (5, 10, 25 kPa): 0.91±0.04; 0.94±0.02; 0.93±0.01). The higher fidelity of the pattern edges becomes evident when we compare profile scans across the average of 150 patterns for both methods to the theoretical pattern shape (Fig 3C and 3D; similar to methods by Vignaud and colleagues [9]). The variation in the protein signal at the pattern edges is strongly reduced in the LOP patterns. These results are also supported by a cross-correlation analysis where we tested the variability and yield of acceptable features across about 400 total feature samples for each gel formulation. We applied a correlation coefficient threshold for acceptable features of 0.84 to match the lowest correlation coefficient in our analysis above. LOP resulted in a greater number of acceptable features than μCP and acceptable feature yield varied from 59% to 98% for LOP and from 4% to 72% for μCP for different gel formulations (see S2 Fig and S2 Table for summary of data).

We demonstrate that single cells as well as pairs of cells attach exclusively to the ECM patterned areas of PAAm gels patterned using the LOP method (Fig 4A and 4B; S1 and S2 Movies). Areas between patterns exhibit anti-adhesive properties and prevent cells from binding outside the protein features. To test if the cytoskeletal architecture and remodeling are

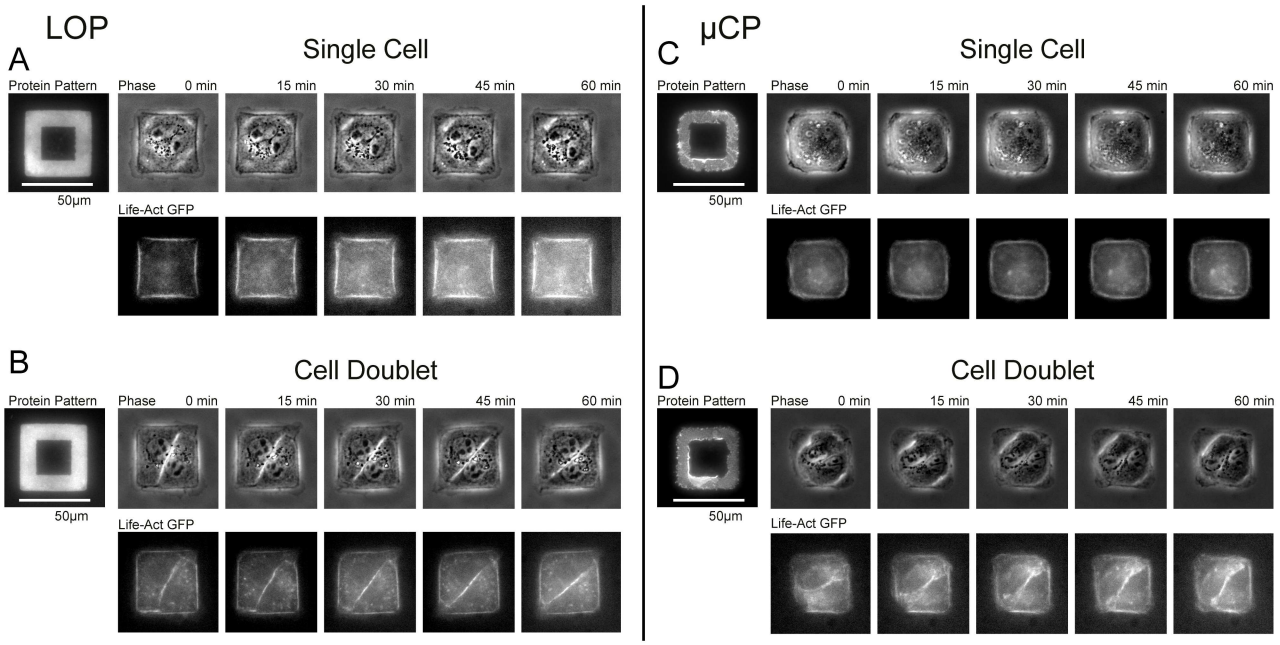

Fig 4. LOP yields sharper cell edges with localized actin bundles compared to μCP patterned gels. Time-lapse acquisitions of MDCK cells transfected with Lifeact-GFP (actin label) grown on 25 kPa PAAm gels showed similar intracellular actin structures on LOP (A, B) and μCP (C,D) protein patterns. Cell doublets rotated around each other on the patterns for both techniques (B,D).

https://doi.org/10.1371/journal.pone.0189901.g004

different for cells attached to patterns created by LOP or μCP, we followed the actin dynamics of LifeAct-GFP transfected MDCK cells using live cell fluorescence microscopy on 25 kPa substrates. We chose to conduct our analysis on gels with a 25 kPa elastic modulus because this value is close to the measured stiffness of a MDCK monolayer by micro-indentation: 33 ± 3 kPa [36]. Consistent with previous literature reports [37], we found that cell doublets on the frame patterns rotated around each other (Fig 4B and 4D; S2–S4 Movies). While this was observed independent of the patterning method used, the cell edges were more clearly defined for cells adhering to patterns created by LOP than gels patterned by μCP (Fig 5), which was consistent with the higher pattern accuracy (Fig 3).

Discussion

In this work, we introduce a photoresist-based LOP technique to pattern ECM proteins on polyacrylamide hydrogels to control the shape of cells with high-fidelity and compare it with the widely used μCP protocol. We found the LOP method to be more efficient and accurate in reproducing complex micrometer-sized patterns (Figs 2 and 3). To illustrate that the improved fidelity of LOP patterns translates to greater control over cell shape, we cultured MDCK epithelial cells on patterned 25 kPa gels for up to 16 hours. The shape of single cells and cell pairs on LOP pattern reflected the theoretical shape with greater accuracy as compared to cells on μCP patterns (Figs 4 and 5; S1–S4 Movies).

The difference between μCP and LOP protein transfer efficiency is most likely arising from how the two methods change substrate surface energy to facilitate protein adsorption. Protein transfer in μCP is based on surface energy differences between the PDMS stamp and the glass substrate [38]. PDMS is hydrophobic with low free energy (water contact angle 91–111˚) while plasma-treated or Hellmanex-cleaned glass is a high-energy hydrophilic surface (contact angle

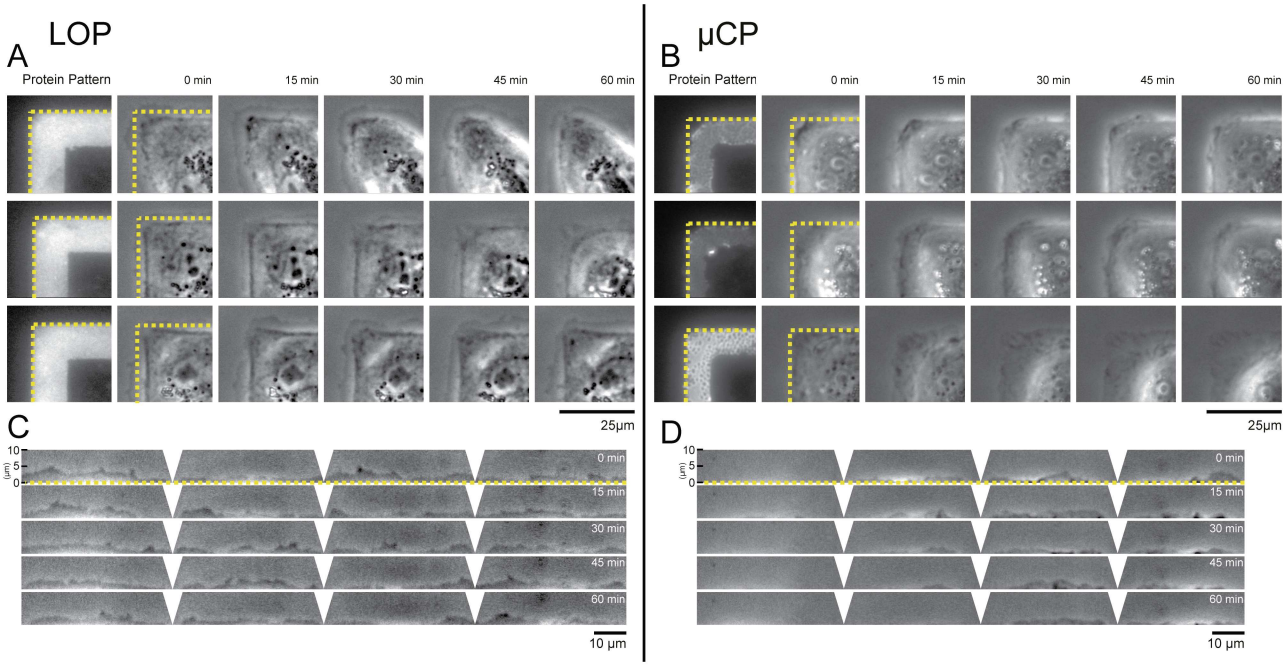

Fig 5. Lamellipodia are more exploratory for cells on LOP than on μCP patterned substrates. Phase contrast time lapse imaging of 3 representative MDCK cells on 25 kPa PAAm gels patterned by LOP (A) and μCP (B). Cells on substrates produced by LOP follow the protein pattern border more accurately (dotted line panels A, B) and reveal more pronounced lamellipodia. (C, D) Kymograph analysis of lamellipodia kinetics along pattern edge. Single cell on LOP pattern shows increased lamellipodia protrusions and retractions within a 10 μm wide region of interest outside the protein pattern edge compared to a cell on a μCP pattern (S5 and S6 Movies). Kymographs show cells depicted in bottom row of panel A and B. Regions of interest are straightened and distorted regions at the pattern corners are cleared.

https://doi.org/10.1371/journal.pone.0189901.g005

of 0˚) (S3 Fig). The hydrophobicity of PDMS causes proteins to denature and lose their conformation thereby decreasing the μCP protein transfer to the glass and to the polyacrylamide gel. In contrast, LOP does not depend on a surface energy gradient and none of the substrates involved in LOP are hydrophobic. We found that the glass had hydrophilic properties at all stages of the LOP protocol with water contact angle of 29–36˚ (see S3 Fig).

Another difference between the protocols which can lead to differences in protein transfer to the PAAm gels is the drying of the PDMS stamp after protein incubation in the μCP protocol. Drying the protein-inked stamp is essential for μCP to be successful to maintain the gradient in surface energy to increase affinity of the adsorbed protein for the hydrophilic glass and to ensure accurate patterning without blurring by diffusion [38]. Yet, drying the protein leads to changes in protein conformation, causing some protein to irreversibly adsorb to the substrate [39]. Experiments which increased the hydrophilicity of PDMS stamps found that the quality of μCP protein transfer decreased due to the presence of polar functional groups attracting the protein to the PDMS rather than the desired glass substrate [40].

The differences in pattern fidelity on the hydrogels stem from methodological differences in the patterning of the glass coverslips. LOP relies on the direct molecular assembly of the biopassive PLL-g-PEG copolymer on the S1818 photoresist-patterned glass substrates while μCP involves PDMS replica molding from SU-8 master structures and stamping of the protein to the coverslip. The ideal spatial resolution that is achievable by contact photolithography to prepare both the S1818 patterns for LOP and the SU-8 master for μCP can be estimated using the following relation between the ideal spatial resolution (R), exposure wavelength (λ) and the

photoresist thickness (z) [41]:

$$R = 1.5 * \sqrt{\lambda \frac{z}{2}}$$

Thus, differences in resist thickness substantially contributes to a decrease in pattern accuracy. We use a 2 μm positive S1818 resist layer for LOP and a 9 μm negative SU-8 resist layer for the fabrication of the PDMS μCP master structures because the resists serve different purposes for each method. The thin positive resist in LOP can be removed by NMP lift-off while keeping the adsorbed PLL-g-PEG as a patterned, biopassive adlayer on the glass coverslip. 9 μm thick negative resist was chosen to yield PDMS feature heights that comply with μCP design rules by Qin and colleagues [42] who suggest that the aspect ratio of a 10:1 Sylgard 184 PDMS stamp must be $0.5 < H/L < 5$ and $H/D > 0.05$, where H is the height of PDMS features, L is the critical feature dimension (line width L = 9 μm for 45μm^2 frame pattern used in this study), and D is the longest distance between features (D = 120 μm, diagonal distance between frame pattern corners). Those design rules avoid lateral pairing and buckling of stamp features, as well as stamp roof collapse to yield successful protein transfer. In contrast to μCP, LOP enables the design and fabrication of arbitrary pattern geometry and spatial organization (e.g. large pattern-to-pattern distance) as it circumvents the PDMS stamping. Additional sources for error in μCP can arise from non-uniform contact of the stamp with the glass coverslip.

In addition to the resist layer thickness, the type of resist used in both protocols further contributes to pattern fidelity. Positive resist has a higher contrast ($\gamma = 2.2$) as compared to negative resist ($\gamma = 1.5$) [43]. This difference contributes to positive resist usually yielding higher resolution features with less distortion than negative resist. The negative SU8 resist used in μCP to create the PDMS mold is also typically under-developed and thus resolving the edges of features is a challenge (see S1 Fig) which explains why μCP results in features which are smaller than the theoretical specifications (see Fig 3A). LOP uses the positive S1818 resist which tends to be over-developed and thus features fabricated by this method tend to be larger than theoretical specifications but with better-resolved corners (see Fig 3A).

We found the lamellipodia of MDCK cells to be more exploratory and dynamic on LOP than μCP substrates, extending up to 5 μm outside of the protein pattern (Fig 5). Epithelial cells have been shown to extend lamellipodia for several micrometers past areas with ECM during wound healing and cell migration [44, 45]. Our observations of lamellipodia extending up to 5 μm beyond adhesive regions and the pronounced actin bundles at the pattern edges match well with the spatio-temporal organization of the cytoskeleton and focal adhesions at the leading edge of migrating cells [46]. Recently, it was shown that epithelial cells migrating from clusters respond to geometrical constraints by altering their speed and that the acto-myosin contractile ring structures of leader cells differ at near sharp corners to help polarize and guide the direction of migration [47]. We were interested to note the dynamic way cells explored LOP patterns due to the increased pattern fidelity on the pattern edges and sharp corners. We thus expect the LOP method to enable future studies on the role of ECM organization on cell migration and lamellipodia extension during embryonic development and cancer metastasis.

An open question for patterns created by LOP is whether the PLL-g-PEG blocking agent on the glass coverslips is transferred to the PAAm gel. In control experiments, we used TRITC-labeled PLL-g-PEG and we were not able to trace fluorescently labeled PLL-g-PEG transferring to the gels nor did we record any loss of TRITC-labeled PLL-g-PEG on the glass coverslip after using it for gel polymerization (see S4 Fig). Additionally, the water contact angle for PLL-g-

PEG coated glass before and after gel polymerization remained constant. This data strongly suggests that the PLL-g-PEG does not transfer from the glass to the gel during gel polymerization. Yet, it remains open if any interactions of PLL-g-PEG copolymer and polyacrylamide occur during gel polymerization. Further molecular level studies are needed to directly test this hypothesis and are outside the scope of this work. Regardless of PLL-g-PEG transfer to the PAAm surface, LOP results in functionalized PAAm gels with non-adhesive regions between protein patterns. We noted that removing the glass coverslips from polymerized gels was easier for samples created by LOP than for μCP (Fig 1G) and we hypothesize that this effect is due to the high water content of the PLL-g-PEG adlayer on the coverslips [48] (see also contact angle data in S3 and S4 Figs).

Conclusions

In summary, our LOP method facilitates advanced cell culture techniques that require precise patterning of single or multiple cells into shapes of arbitrary geometry on PAAm hydrogel substrates of varied stiffness. High pattern accuracy and defined ECM density within the protein patterns are essential to compare cell phenotypes on different patterns and reduce the systematic error of pooled measurements. This is of particular importance for studies focusing on complex, multivariate cell-ECM signaling pathways and the cytoskeletal response to different cell geometries and substrate stiffness [49]. Overall, local ECM density, cell shape, and substrate stiffness have been shown to regulate the structural organization of focal adhesion complexes [50, 51], the force balance between cell-cell and cell-ECM adhesions [4], the nuclear lamina [52], mesenchymal stem cell stiffness [53], stem cell fate [12, 54], leader cells during collective migration [47], and the contractile properties of cardiomyocytes [55].

Supporting information

S1 Table. Polyacrylamide gel formulations used in this study.
(DOCX)

S2 Table. Acceptable feature yield results.
(DOCX)

S1 Text. File with detailed protocols for the microcontact printing and lift-off methods. We also include comparisons between polyacrylamide pore size and gelatin protein molecular size to aid discussion of protein transfer efficiency.
(DOCX)

S1 Fig. Overview of the SU8 master and PDMS stamps used for microcontact printing. The photolithography mold (A) and PDMS stamp cast from this mold (B) show rounded corners where the edges of the pattern meet, both in the inner and outer regions of the pattern. The height of the SU8 mold (~9 μm) may be limiting the pattern accuracy achievable with microcontact printing.
(TIF)

S2 Fig. LOP results in higher yield of acceptable features than μCP. By setting a threshold of a 0.84 correlation coefficient, the LOP protocol resulted in more acceptable features than μCP (highlighted in green). We selected 389–416 features for each gel sample and then performed cross correlation analysis on the collected feature montage. Acceptable feature yield varied from 59% to 98% for LOP and from 4% to 72% for μCP for different gel formulations. See S2 Table for summary of data.
(TIF)

S3 Fig. μCP depends on surface energy differences while substrates used for LOP have similar surface energies. The water contact angle of substrates used in μCP differs substantially from average of 111˚ for PDMS (n = 12 measurements) to approximately 0˚ for Hellmanex-cleaned glass (the substrate used for μCP). The Hellmanex treated glass sample was super hydrophilic making an exact measurement of the low water contact angle difficult. Untreated glass is shown as comparison with an average water contact angle 75˚ (n = 8 measurements). The substrates used for LOP varied little in water contact angle. The "UV-exposed" sample corresponds to glass cleaned with acetone-isopropanol-water, coated with S1818 resist, flood-exposed to UV, developed, and processed with NMP for lift-off. In the LOP protocol, areas that adsorb the PLL-g-PEG adlayer have been treated with the same procedure. The "masked" sample corresponds to glass cleaned with acetone-isopropanol-water, coated with S1818 resist, no UV exposure, developed, and processed with NMP for lift-off. This substrate thus replicates the surface areas that adsorb protein in the LOP protocol. See insets from our LOP protocol and mask design for clarification. We recorded average water contact angles of 36˚ for glass cleaned in a series of acetone-isopropanol-water (n = 48 measurements), 34˚ for "UV exposed" samples (n = 38 measurements), and 29˚ for "masked" samples (n = 12 measurements).
For μCP, protein must be transferred from the hydrophobic PDMS to the hydrophilic Hellmanex-cleaned glass. For LOP, protein would be adsorbed to the areas masked by S1818 after those areas are exposed by lift-off and we found these areas to be hydrophilic. Insets show examples of water droplets on the corresponding substrates.
(TIF)

S4 Fig. PLL-g-PEG remains on the glass slide after gel polymerization due to similar water contact angle before and after gel polymerization and using a fluorescent PLL-g-PEG. A.) We measured the contact angle of PLL-g-PEG coated glass before and after polymerizing a polyacrylamide gel. The average water contact angle is similar with 27˚ for PLL-g-PEG glass (n = 46 measurements) and 23˚ for PLL-g-PEG glass after gel polymerization (n = 42 measurements). B.) We also used TRITC-labeled PLL-g-PEG on the LOP patterned glass and measured the intensity of the fluorescent signal before and after gel polymerization on the same coverslip. We show a representative image showing the PLL-g-PEG-TRITC signal outside of the protein features (dark frames in image). We subtracted the signal within the protein pattern areas and divided the average PLL-g-PEG-TRITC signal 'after' gel polymerization by the 'before' signal. Within the limits of the measurement, no loss in PLL-g-PEG-TRITC intensity on the glass coverslip was observed (average 98% ± 2.6% of the initial signal remains on the glass after gel polymerization, n = 80 regions analyzed). We were also unable to detect PLL-g-PEG on the surface of the resulting polyacrylamide gels. Together, our water contact angle and fluorescence imaging data strongly suggest that PLL-g-PEG is not transferred to the PAAm gel during LOP.
(TIF)

S1 Movie. Single MDCK on LOP gel. Three separate time-lapse acquisitions (5 minute increments, time shown at upper left) of single MDCK cells on LOP-functionalized 25 kPa PAAm gels. Three channels are shown (gelatin for protein patterning, phase for cell outline, and LifeAct-GFP for actin structures). Scale bar is 45 μm wide.
(MP4)

S2 Movie. Doublet MDCK cell pairs on LOP gel. Three separate time-lapse acquisitions (5 minute increments, time shown at upper left) doublet MDCK cell pairs on LOP-functionalized 25 kPa PAAm gels. Three channels are shown (gelatin for protein patterning, phase for cell

outline, and LifeAct-GFP for actin structures). Scale bar is 45 μm wide.
(MP4)

S3 Movie. Single MDCK on μCP gel. Three separate time-lapse acquisitions (5 minute increments, time shown at upper left) of single MDCK cells on μCP-functionalized 25 kPa PAAm gels. Three channels are shown (gelatin for protein patterning, phase for cell outline, and LifeAct-GFP for actin structures). Scale bar is 45 μm wide.
(MP4)

S4 Movie. Doublet MDCK cell pairs on μCP gel. Three separate time-lapse acquisitions (5 minute increments, time shown at upper left) doublet MDCK cell pairs on μCP-functionalized 25 kPa PAAm gels. Three channels are shown (gelatin for protein patterning, phase for cell outline, and LifeAct-GFP for actin structures). Scale bar is 45 μm wide.
(MP4)

S5 Movie. Lamellipodia beyond pattern edge for a cell on LOP gel. A time-lapse acquisition (5 minute increments, time shown at upper left) of an MDCK cell lamellipodia extending past the protein pattern region created by LOP. The image is a 'straightened' path along the cell edge (on bottom) extending 10 μm past the protein pattern (away from the cell). Scale bar is 10 μm wide.
(MP4)

S6 Movie. Lamellipodia beyond pattern edge for a cell on μCP gel. A time-lapse acquisition (5 minute increments, time shown at upper left) of an MDCK cell lamellipodia extending past the protein pattern region created by μCP. The image is a 'straightened' path along the cell edge (on bottom) extending 10 μm past the protein pattern (away from the cell). Scale bar is 10 μm wide.
(MP4)

Acknowledgments

The authors thank Pruitt lab members for helpful discussion of results and Dr. Jeffrey Tok from the Stanford Soft and Hybrid Materials Facility for his advice on characterizing substrates using the contact angle goniometer.

Author Contributions

Conceptualization: Jens Moeller, Aleksandra K. Denisin, Alexandre J. S. Ribeiro, Beth L. Pruitt.

Data curation: Jens Moeller, Aleksandra K. Denisin.

Formal analysis: Jens Moeller, Aleksandra K. Denisin.

Funding acquisition: Beth L. Pruitt.

Investigation: Jens Moeller, Aleksandra K. Denisin, Joo Yong Sim, Robin E. Wilson, Alexandre J. S. Ribeiro.

Methodology: Jens Moeller, Aleksandra K. Denisin, Joo Yong Sim, Robin E. Wilson, Alexandre J. S. Ribeiro.

Project administration: Beth L. Pruitt.

Resources: Beth L. Pruitt.

Supervision: Beth L. Pruitt.

Visualization: Jens Moeller, Aleksandra K. Denisin.

Writing – original draft: Jens Moeller, Aleksandra K. Denisin, Beth L. Pruitt.

Writing – review & editing: Jens Moeller, Aleksandra K. Denisin, Joo Yong Sim, Robin E. Wilson, Alexandre J. S. Ribeiro, Beth L. Pruitt.

References

1. Théry M. Micropatterning as a tool to decipher cell morphogenesis and functions. J Cell Sci. 2010; 123 (Pt 24):4201–13. https://doi.org/10.1242/jcs.075150 PMID: 21123618.
2. Tse JR, Engler AJ. Preparation of hydrogel substrates with tunable mechanical properties. Curr Protoc Cell Biol. 2010; 47(10):Unit 10.6. https://doi.org/10.1002/0471143030.cb1016s47 PMID: 20521229.
3. Kassianidou E, Kumar S. A biomechanical perspective on stress fiber structure and function. Biochim Biophys Acta. 2015; 1853(11 Pt B):3065–74. https://doi.org/10.1016/j.bbamcr.2015.04.006 PMID: 25896524.
4. Sim JY, Moeller J, Hart KC, Ramallo D, Vogel V, Dunn AR, et al. Spatial Distribution of Cell-Cell and Cell-ECM Adhesions Regulates Force Balance while Maintaining E-cadherin Molecular Tension in Cell Pairs. Mol Biol Cell. 2015; 26(13):2456–65. https://doi.org/10.1091/mbc.E14-12-1618 PMID: 25971797.
5. Ribeiro AJS, Denisin AK, Wilson RE, Pruitt BL. For whom the cells pull: Hydrogel and micropost devices for measuring traction forces. Methods. 2016; 94:51–64. https://doi.org/10.1016/j.ymeth.2015.08.005 PMID: 26265073.
6. Grevesse T, Versaevel M, Circelli G, Desprez S, Gabriele S. A simple route to functionalize polyacrylamide hydrogels for the independent tuning of mechanotransduction cues. Lab Chip. 2013; 13(5):777–80. https://doi.org/10.1039/c2lc41168g PMID: 23334710.
7. Rape AD, Guo W-H, Wang Y-l. The regulation of traction force in relation to cell shape and focal adhesions. Biomaterials. 2011; 32(8):2043–51. https://doi.org/10.1016/j.biomaterials.2010.11.044 PMID: 21163521.
8. Polio SR, Parameswaran H, Canović EP, Gaut CM, Aksyonova D, Stamenović D, et al. Topographical control of multiple cell adhesion molecules for traction force microscopy. Integrative Biology. 2014; 6 (3):357–65. https://doi.org/10.1039/c3ib40127h PMID: 24441735.
9. Vignaud T, Ennomani H, Théry M. Polyacrylamide Hydrogel Micropatterning. Methods Cell Biol. 120: Elsevier; 2014. p. 93–116. https://doi.org/10.1016/B978-0-12-417136-7.00006-9 PMID: 24484659
10. Alom Ruiz S, Chen CS. Microcontact printing: A tool to pattern. Soft Matter. 2007; 3(2):168–77. https://doi.org/10.1039/B613349E
11. Qin D, Xia Y, Whitesides GM. Soft lithography for micro- and nanoscale patterning. Nat Protoc. 2010; 5 (3):491–502. https://doi.org/10.1038/nprot.2009.234 PMID: 20203666.
12. Lee J, Abdeen AA, Zhang D, Kilian KA. Directing stem cell fate on hydrogel substrates by controlling cell geometry, matrix mechanics and adhesion ligand composition. Biomaterials. 2013; 34(33):8140–8. https://doi.org/10.1016/j.biomaterials.2013.07.074 PMID: 23932245.
13. Tang X, Ali MY, Saif MTA. A Novel Technique for Micro-patterning Proteins and Cells on Polyacrylamide Gels. Soft Matter. 2012; 8(27):7197–206. https://doi.org/10.1039/C2SM25533B PMID: 23002394.
14. Hui CY, Jagota A, Lin YY, Kramer EJ. Constraints on microcontact printing imposed by stamp deformation. Langmuir. 2002; 18:1394–407. https://doi.org/10.1021/la0113567
15. Huang YY, Zhou W, Hsia KJ, Menard E, Park J-U, Rogers JA, et al. Stamp Collapse in Soft Lithography. Langmuir. 2005; 21(17):8058–68. https://doi.org/10.1021/la0502185 PMID: 16089420
16. Delamarche E, Schmid H, Michel B, Biebuyck HA. Stability of molded polydimethylsiloxane microstructures. Advanced Materials. 1997; 9:741–6.
17. Park TH, Shuler ML. Integration of cell culture and microfabrication technology. Biotechnol Prog. 2003; 19(2):243–53. https://doi.org/10.1021/bp020143k PMID: 12675556.
18. Masters T, Engl W, Weng ZL, Arasi B, Gauthier N, Viasnoff V. Easy Fabrication of Thin Membranes with Through Holes. Application to Protein Patterning. PLoS One. 2012; 7(8):e44261–7. https://doi.org/10.1371/journal.pone.0044261 PMID: 22952944

19. Chen W, Lam RHW, Fu J. Photolithographic surface micromachining of polydimethylsiloxane (PDMS). Lab Chip. 2012; 12(2):391–5. https://doi.org/10.1039/c1lc20721k PMID: 22089984.

20. Desai RA, Rodriguez NM, Chen CS. "Stamp-off" to micropattern sparse, multicomponent features. Methods Cell Biol. 2014; 119:3–16. https://doi.org/10.1016/B978-0-12-416742-1.00001-9 PMID: 24439276.

21. Christman KL, Enriquez-Rios VD, Maynard HD. Nanopatterning proteins and peptides. Soft Matter. 2006; 2(11):928–12. https://doi.org/10.1039/b611000b

22. Narui Y, Salaita KS. Dip-pen nanolithography of optically transparent cationic polymers to manipulate spatial organization of proteolipid membranes. Chem Sci. 2012; 3(3):794–9.

23. Wagner MS, Pasche S, Castner DG, Textor M. Characterization of poly(L-lysine)-graft-poly(ethylene glycol) assembled monolayers on niobium pentoxide substrates using time-of-flight secondary ion mass spectrometry and multivariate analysis. Anal Chem. 2004; 76(5):1483–92. https://doi.org/10.1021/ac034873y PMID: 14987107.

24. Pasche S, De Paul SM, Vöros J, Spencer ND, Textor M. Poly(L-lysine)-graft-poly(ethylene glycol) assembled monolayers on niobium oxide surfaces: A quantitative study of the influence of polymer interfacial architecture on resistance to protein adsorption by ToF-SIMS and in situ OWLS. Langmuir. 2003; 19:9216–25. https://doi.org/10.1021/la034111y

25. Azioune A, Carpi N, Tseng Q, Théry M, Piel M. Protein Micropatterns. A Direct Printing Protocol Using Deep UVs. Methods Cell Biol. 2010; 97(C):133–46. https://doi.org/10.1016/S0091-679X(10)97008-8 PMID: 20719269.

26. Strale P-O, Azioune A, Bugnicourt G, Lecomte Y, Chahid M, Studer V. Multiprotein Printing by Light-Induced Molecular Adsorption. Adv Mater Weinheim. 2016; 28(10):2024–9. https://doi.org/10.1002/adma.201504154 PMID: 26689426.

27. Falconnet D, Pasqui D, Park S, Eckert R, Schift H, Gobrecht J, et al. A Novel Approach to Produce Protein Nanopatterns by Combining Nanoimprint Lithography and Molecular Self-Assembly. Nano Lett. 2004; 4(10):1909–14. https://doi.org/10.1021/nl0489438

28. Fredericks EC, Kotecha HN, inventors; United States Patent, assignee. Photoresist lift-off process for fabricating semiconductor devices. United States patent US 06/567,034. 1986 Feb 14.

29. Falconnet D, Koenig A, Assi F, Textor M. A Combined Photolithographic and Molecular-Assembly Approach to Produce Functional Micropatterns for Applications in the Biosciences. Adv Funct Mater. 2004; 14(8):749–56. https://doi.org/10.1002/adfm.200305182

30. Anderegg F, Geblinger D, Horvath P, Charnley M, Textor M, Addadi L, et al. Substrate adhesion regulates sealing zone architecture and dynamics in cultured osteoclasts. PLoS One. 2011; 6(12):e28583. https://doi.org/10.1371/journal.pone.0028583 PMID: 22162778.

31. Moeller J, Emge P, Avalos Vizcarra I, Kollmannsberger P, Vogel V. Bacterial filamentation accelerates colonization of adhesive spots embedded in biopassive surfaces. New J Phys. 2013; 15(12):125016. https://doi.org/10.1088/1367-2630/15/12/125016 related:A02FwzaWv6kJ.

32. Zhu J, Marchant RE. Design properties of hydrogel tissue-engineering scaffolds. Expert Rev Med Devices. 2011; 8(5):607–26. https://doi.org/10.1586/erd.11.27 PMID: 22026626.

33. Guo W-H, Wang Y-l. Micropatterning cell-substrate adhesions using linear polyacrylamide as the blocking agent. Cold Spring Harb Protoc. 2011; 2011(3):prot5582. https://doi.org/10.1101/pdb.prot5582 PMID: 21363946.

34. Tseng Q, Wang I, Duchemin-Pelletier E, Azioune A, Carpi N, Gao J, et al. A new micropatterning method of soft substrates reveals that different tumorigenic signals can promote or reduce cell contraction levels. Lab Chip. 2011; 11(13):2231. https://doi.org/10.1039/c0lc00641f PMID: 21523273.

35. Stalder AF, Kulik G, Sage D, Barbieri L, Hoffmann P. A snake-based approach to accurate determination of both contact points and contact angles. Colloids and surfaces A, Physicochemical and engineering aspects. 2006; 286(1–3):92–103. https://doi.org/10.1016/j.colsurfa.2006.03.008

36. Schulze KD, Zehnder SM, Urueña JM, Bhattacharjee T, Sawyer WG, Angelini TE. Elastic modulus and hydraulic permeability of MDCK monolayers. J Biomech. 2017. https://doi.org/10.1016/j.jbiomech.2017.01.016 PMID: 28173919.

37. Tseng Q, Duchemin-Pelletier E, Deshiere A, Balland M, Guillou H, Filhol O, et al. Spatial organization of the extracellular matrix regulates cell–cell junction positioning. Proc Natl Acad Sci U S A. 2012; 109(5):1506–11. https://doi.org/10.1073/pnas.1106377109 PMID: 22307605

38. Ricoult SG, Sanati Nezhad A, Knapp-Mohammady M, Kennedy TE, Juncker D. Humidified Microcontact Printing of Proteins: Universal Patterning of Proteins on Both Low and High Energy Surfaces. Langmuir. 2014; 30(40):12002–10. https://doi.org/10.1021/la502742r PMID: 25222734

39. Kaufmann T, Ravoo BJ. Stamps, inks and substrates: polymers in microcontact printing. Polymer Chemistry. 2010; 1(4):371–17. https://doi.org/10.1039/b9py00281b

40. Tan JL, Tien J, Chen CS. Microcontact printing of proteins on mixed self-assembled monolayers. Langmuir. 2002; 18(2):519–23. https://doi.org/10.1021/la011351+

41. Madou MJ. Manufacturing Techniques for Microfabrication and Nanotechnology. 3 ed: CRC Press; 2011.

42. Qin D, Xia Y, Whitesides GM. Soft lithography for micro- and nanoscale patterning. Nat Protoc. 2010; 5(3):491–502. https://doi.org/10.1038/nprot.2009.234 PMID: 20203666.

43. Madou PM, Wang PC. Photolithography. Dordrecht: Springer Netherlands; 2012. p. 2051–60.

44. Das T, Safferling K, Rausch S, Grabe N, Boehm H, Spatz JP. A molecular mechanotransduction pathway regulates collective migration of epithelial cells. Nat Cell Biol. 2015; 17(3):276–87. https://doi.org/10.1038/ncb3115 PMID: 25706233.

45. Ravasio A, Cheddadi I, Chen T, Pereira T, Ong HT, Bertocchi C, et al. Gap geometry dictates epithelial closure efficiency. Nat Commun. 2015; 6:7683. https://doi.org/10.1038/ncomms8683 PMID: 26158873.

46. Burnette DT, Manley S, Sengupta P, Sougrat R, Davidson MW, Kachar B, et al. A role for actin arcs in the leading-edge advance of migrating cells. Nat Cell Biol. 2011; 13(4):371–81. https://doi.org/10.1038/ncb2205 PMID: 21423177.

47. Kollimada SA, Kulkarni AH, Ravan A, Gundiah N. Advancing Edge Speeds of Epithelial Monolayers Depend on Their Initial Confining Geometry. PLoS One. 2016; 11(4):e0153471. https://doi.org/10.1371/journal.pone.0153471 PMID: 27078632.

48. Pasche S, Vöros J, Griesser HJ, Spencer ND, Textor M. Effects of ionic strength and surface charge on protein adsorption at PEGylated surfaces. J Phys Chem B. 2005; 109(37):17545–52. https://doi.org/10.1021/jp050431+ PMID: 16853244.

49. Tseng P, Di Carlo D. Substrates with Patterned Extracellular Matrix and Subcellular Stiffness Gradients Reveal Local Biomechanical Responses. Adv Mater Weinheim. 2014; 26(8):1242–7. https://doi.org/10.1002/adma.201304607 PMID: 24323894

50. Balaban NQ, Schwarz US, Riveline D, Goichberg P, Tzur G, Sabanay I, et al. Force and focal adhesion assembly: a close relationship studied using elastic micropatterned substrates. Nat Cell Biol. 2001; 3(5):466–72. https://doi.org/10.1038/35074532 PMID: 11331874.

51. Cavalcanti-Adam EA, Volberg T, Micoulet A, Kessler H, Geiger B, Spatz JP. Cell Spreading and Focal Adhesion Dynamics Are Regulated by Spacing of Integrin Ligands. Biophys J. 2007; 92(8):2964–74. https://doi.org/10.1529/biophysj.106.089730 PMID: 17277192

52. Ihalainen TO, Aires L, Herzog FA, Schwartlander R, Moeller J, Vogel V. Differential basal-to-apical accessibility of lamin A/C epitopes in the nuclear lamina regulated by changes in cytoskeletal tension. Nat Mater. 2015; 14(12):1252–61. https://doi.org/10.1038/nmat4389 PMID: 26301768.

53. Tee S-Y, Fu J, Chen CS, Janmey PA. Cell Shape and Substrate Rigidity Both Regulate Cell Stiffness. Biophys J. 2011; 100(5):L25–L7. https://doi.org/10.1016/j.bpj.2010.12.3744 PMID: 21354386

54. Trappmann B, Gautrot JE, Connelly JT, Strange DGT, Li Y, Oyen ML, et al. Extracellular-matrix tethering regulates stem-cell fate. Nat Mater. 2012; 11(7):642–9. https://doi.org/10.1038/nmat3339 PMID: 22635042.

55. Ribeiro AJ, Ang YS, Fu JD, Rivas RN, Mohamed TM, Higgs GC, et al. Contractility of single cardiomyocytes differentiated from pluripotent stem cells depends on physiological shape and substrate stiffness. Proc Natl Acad Sci U S A. 2015; 112(41):12705–10. https://doi.org/10.1073/pnas.1508073112 PMID: 26417073.